Published in : Colloids and Surfaces A: Physicochemical and Engineering Aspects (2020), vol. 606, 125390
DOI: https://doi.org/10.1016/j.colsurfa.2020.125390
Status : Postprint (Author's version)

CARBON-COATED POROUS TiO_2 LAYERS TEMPLATED BY CORE-SHELL POLYMER PARTICLES : FILM PROCESSING AND CHARGE TRANSFER RESISTANCE ASSESSMENT

Vidhyadevi Thangaraj[a], Jennifer Dewalque[b], Anthony Maho[b], Gilles Spronck[b], Cédric Malherbe[c], Abdelhafid Aqil[a], Rudi Cloots[b], Pierre Colson[b], Christine Jérôme[a], Antoine Debuigne[a]

[a] *Center for Education and Research on Macromolecules (CERM), CESAM Research Unit, Chemistry Department, University of Liège (ULiège), Quartier Agora, 13 Allée du Six Août (Bldg B6a), Sart-Tilman, B-4000 Liège, Belgium*
[b] *Group of Research in Energy and Environment from Materials (GREEnMat), CESAM Research Unit, Chemistry Department, University of Liège (ULiège), Quartier Agora, 13 Allée du Six Août (Bldg B6a), Sart-Tilman, B-4000 Liège, Belgium*
[c] *Laboratory of Mass Spectrometry, Molsys Research Unit, Chemistry Department, University of Liège (ULiège), Quartier Agora, 13 Allée du Six Août (Bldg B6d), Sart-Tilman, B-4000 Liège, Belgium*

KEYWORDS : Porous TiO_2 films ; Core-shell particle templates; Anatase TiO_2; Conductive carbon coating ; Charge transfer properties

ABSTRACT :

The performances of titanium dioxide (TiO_2) thin films used in photoelectrochemical applications (solar cells, water splitting, photocatalysis, etc) highly depend on their morphology and interface. In this work, we describe a straightforward strategy for designing conductive carbon-coated TiO_2 porous layers allowing for the tuning of interfacial charge transfers. Increased specific surface and improved conductivity are expected from the porosity and the carbon coating, respectively. In practice, polystyrene/polyacrylonitrile (PS-PAN) and polystyrene/ polydopamine (PS-PDA) core-shell particles synthesized by emulsion polymerization are considered as templating agents for the production of carbon-coated and ordered porous TiO_2 layers. After spin coating deposition of the particles, infiltration of the TiO_2 precursor and calcination, voids are created in the film by thermal degradation of the PS cores whereas PAN and PDA produced carbon at the surface of the TiO_2 inverse opal matrix. Uncoated PS particles are also considered as benchmark templating agents. Size and composition of the polymer particles as well as the morphology and electronic properties of the corresponding porous TiO_2 films are evaluated. In particular, the charge transfer resistance of the films is investigated via Electrochemical Impedance Spectroscopy (EIS) as a preliminary assessment of these unprecedented carbon-coated porous TiO_2 layers as semiconducting materials.

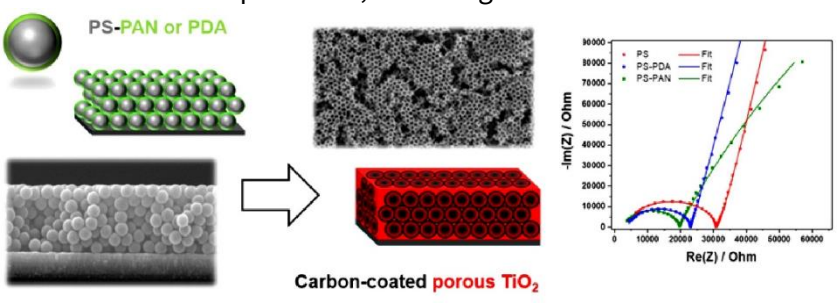

Published in : Colloids and Surfaces A: Physicochemical and Engineering Aspects (2020), vol. 606, 125390
DOI: https://doi.org/10.1016/j.colsurfa.2020.125390
Status : Postprint (Author's version)

1. Introduction

In the last decades, titanium oxide-based materials raised huge interest in many fields like energy conversion [1] and storage [2], photocatalysis [3,4], or design of electronic devices and sensors [5] due to their low cost, high physicochemical stability, non-toxicity and suitable band gap energy. Several nanostructured TiO_2 morphologies have been investigated throughout literature so to emphasize the significant impact of the structural dimensionality of TiO_2 on its properties and performances. The morphological and structural tuning of such porous titania layers towards large interfacial area and adjustable pore shape, size, orientation and interconnectivity, appears to be crucial in terms of their resulting functionality and efficiency [6,7]. To this extent, the use of colloidal templating strategies has been highlighted as advantageous and fruitful [8-10]. This approach is based on the surface assembly of colloidal crystals, usually made of nanospheres of silica SiO_2 or polymers such as polystyrene (PS) or poly(methyl methacrylate) (PMMA), followed by the infiltration of the TiO_2 precursor and the ultimate removal of the beads template through chemical and/or thermal treatment. A large variety of assembly methods have been reported for the corresponding preparation of ordered porous TiO_2 layers such as evaporative, electrophoretic, dip as well as spin coating deposition [11], notably for the getting of TiO_2 inverse opals of interest for photonics [12,13] and solar cells [14-17] applications.

Despite of the multiple advantages of structuring TiO_2 into materials with high surface area, the latter may still suffer from intrinsically poor electrical conductivities, moderate visible light response, low quantum efficiency and limited mass diffusion, which prevents their full exploitation in the applications mentioned above.

One approach to overcome these limitations and improve the optoelectronic properties of TiO_2 consists in combining the metal oxide with a (semi)conductor with a suitable narrow band gap. In this respect, carbon appears to be an interesting additive for TiO_2 due to its ability to conduct electrons and to limit the recombination of the charge carriers. The incorporation of conductive carbon into titanium oxide layers notably led to materials with improved performances in the areas of photocatalysis [18], energy storage in batteries [19,20] and solar cells [21,22], to name only a few. Interestingly, a number of carbon/TiO_2 composites consist in TiO_2 particles coated by carbon via decomposition of organic materials [23-27].

Here, we describe a straightforward strategy for preparing conductive carbon-coated and ordered porous TiO_2 layers involving coreshell polymer particles as both templating agents and source of carbon (Figure 1). For this purpose, PS was chosen as sacrificial core material of the particles whereas polyacrylonitrile (PAN) [28-32] and polydopamine (PDA) [33-37] were selected as outer layer of the core-shell particles due to their ability to generate N-doped conductive carbon under appropriate calcination conditions.

For the sake of the comparison, carbon-free porous TiO_2 layers were also prepared from pristine PS particles. Special care was devoted to study the morphology and electrical properties of the resulting porous films. Electrochemical Impedance Spectroscopy (EIS) measurements notably

Published in : Colloids and Surfaces A: Physicochemical and Engineering Aspects (2020), vol. 606, 125390
DOI: https://doi.org/10.1016/j.colsurfa.2020.125390
Status : Postprint (Author's version)

highlighted the impact on charge transfer properties of the carbon-coated porous TiO_2 layers obtained with the PS-PAN and PS-PDA particles, respectively.

***Figure 1**. Design of carbon-coated porous TiO_2 layers using PS-PAN or PS-PDA core-shell particles.*

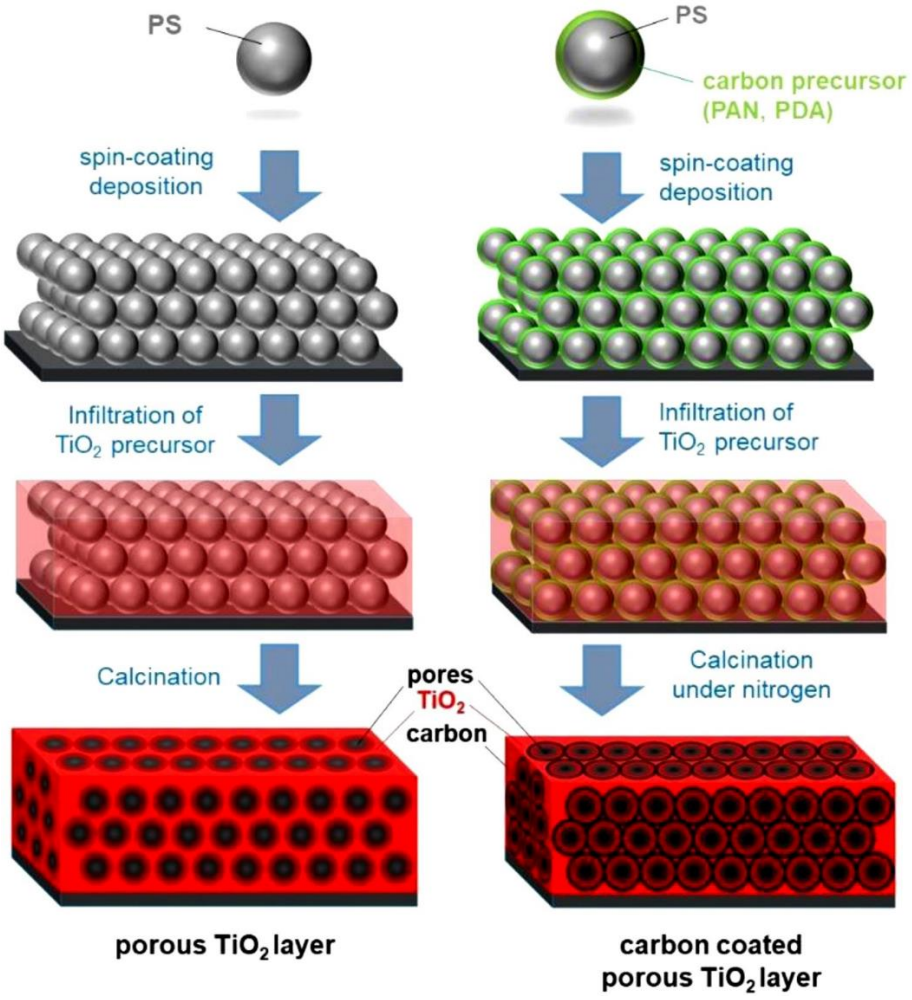

2. Materials and methods

2.1. MATERIALS

Acrylonitrile, dopamine hydrochloride (98 %), potassium persulfate (KPS), isopropanol and absolute methanol were purchased from Sigma Aldrich and used as received. Styrene was purchased from Sigma Aldrich and the inhibitor was removed upon washing with 5 % NaOH aqueous solution. Ultrapure water was produced from Milli-Q plus 188 apparatus (Millipore).

Published in : Colloids and Surfaces A: Physicochemical and Engineering Aspects (2020), vol. 606, 125390
DOI: https://doi.org/10.1016/j.colsurfa.2020.125390
Status : Postprint (Author's version)

2.2. CHARACTERIZATION

Particle size and polydispersity index were determined by dynamic light scattering (DLS) analysis on Delsa Nano C from BECKMAN COULTER instrument. The morphology of the particles was studied by Transmission Electron Microscopy (TEM, CM100 from Philips) with an operating voltage of 80 kV. The morphology of the PS, PS-PAN or PS-PDA particles layers and of the final TiO_2 porous films was examined by Scanning Electron Microscopy (SEM, FEI ESEM XL30 instrument) with an operating voltage of 15 kV. Carbon coating at the surface of the TiO_2 porous matrix was evidenced by Transmission Electron Microscopy (TEM, FEI Tecnai G2 TWIN instrument) with an operating voltage of 200 kV. X-ray diffraction (XRD) data were collected on a Bruker D8 grazing incidence diffractometer with CuK_α radiation. Thermogravimetric analyses (TGA) were performed on a Q500 from TA instrument in order to quantify the amount of residual carbon upon carbonization. The latter was carried out via a three-step procedure, (i) 10 min at 150 °C, (ii) increase of the temperature to 600 °C with a ramp of 20 °C/min, (iii) thermal treatment at 600 °C for 30 min. The nature of the carbon produced upon carbonization of the PS-PAN and PS-PDA particles were measured by Raman spectroscopy using a LabRam 300 confocal Raman spectrometer (Horiba Jobin-Yvon) operated with a 647 nm excitation laser (Krypton laser Spectra Physics 168B). The instrument is interfaced with a microscope Olympus BX40 and a CCD detector (Andor iDus DU401 BR DD). Electrochemical Impedance Spectroscopy (EIS) was conducted in dark conditions at room temperature, using a Biologic SP-200 Potentiostat (Science Instrument) and a three-electrodes setup with the porous TiO_2-covered glass sample as working electrode (active surface of 0.28 cm^2), a Pt foil as counter electrode and a Ag-AgCl reference electrode adapted for non-aqueous media (model REF361 from HACH). The three electrodes were put in contact with a 5 mM tetrabutylammonium perchlorate (TBAClO4) electrolyte in dichloromethane (CH_2Cl_2). After 10 min of N_2 degassing, EIS curves were recorded after 2 min of stabilization at the open circuit potential value in the 2 MHz - 50 mHz frequency range with a 10 mV amplitude. Data were analysed and fitted using EC-Lab software.

2.3. SYNTHESIS OF PARTICLES

PS particles were synthesized via a surfactant-free emulsion polymerization procedure inspired from a similar approach described by Cai et al. [38] Typically, styrene (2.73 g, 26.2 mmol, 3.0 mL) and deionized water (100 mL) were introduced in a two-neck 250 mL round bottomed flask equipped with magnetic stirrer, and addition funnel, an argon gas inlet and a thermostatic oil bath. This mixture was degassed by bubbling with argon at room temperature for 30 min under stirring at 650 rpm. A degassed solution of KPS (70 mg, 0.26 mmol) in 25 mL deionized water was charged in the addition funnel. The styrene mixture was heated at 70 °C before dropwise addition of the KPS aqueous solution. Heating and stirring was then maintained for 24 h leading to an aqueous suspension of PS particles. The latter were purified and isolated by centrifugation, washed three times with methanol and dried under vacuum oven at 50 °C for 24 h.

PS-PAN core-shell particles were prepared by a procedure adapted from a previously reported method [39]. Typically, distilled de-ionized (DDI) water (100 mL) and styrene (50 mmol, 5.2 g, 5.72 mL) were placed in a 250 mL round bottomed flask equipped with a magnetic stirrer, nitrogen inlet,

Published in : Colloids and Surfaces A: Physicochemical and Engineering Aspects (2020), vol. 606, 125390
DOI: https://doi.org/10.1016/j.colsurfa.2020.125390
Status : Postprint (Author's version)

condenser and a pipette outlet for sampling. The mixture was degassed by bubbling nitrogen for 30 min before heating the reaction medium at 70 °C under stirring (650 rpm). When temperature reached 70 °C, a degassed solution of KPS (0.1 mmol, 27 mg) in DDI-water (25 mL) was added dropwise to the mixture and styrene was allowed to polymerize for 30 min at 70 °C under stirring. Next, degassed acrylonitrile (50 mmol, 2.65 g, 3.27 mL) was added dropwise and the reaction was continued for 5 h under stirring at 70 °C, leading to an aqueous suspension of PS-PAN particles. The resulting particles were isolated by centrifugation of the solution, washed three times with methanol and dried under vacuum oven at 50 °C for 24 h.

PS-PDA core-shell particles were synthesized as follows. The abovementioned purified PS particles (250 mg) were dispersed in a Tris-HCl buffer (78 mL, 10 mM, pH 8.5) under sonication. Then, dopamine hydrochloride (DA) (62.5 mg, $DA/PS_{w/w}$ = 0.25) was added to the PS particles suspension and stirred at room temperature for 24 h leading to an aqueous suspension of PS-PDA particles. The resulting particles were collected by centrifugation, rinsed with deionized water three times and dried under vacuum at 50 °C for 24 h.

2.4. SPIN COATING DEPOSITION OF PARTICLES ONTO CONDUCTIVE GLASS

The above-mentioned aqueous suspensions of PS, PS-PAN and PS-PDA (aliquots containing 60 mg of particles) were added with an equal volume of isopropanol in order to destabilize the suspension and isolate the particles. The mixture was centrifuged at 12,000 rpm for 20 min and supernatant was eliminated. Particles were then suspended in a H2O/ isopropanol mixture (360 µL, $V_{H2O}/V_{isopropanol}$: 1/3) before being homogenized by vortex stirring and ultrasonic bath (cooled by ice) in order to get the desired 15 w/v % particle suspensions. Beads suspensions (160 µL) were then deposited on 2 × 2 cm FTO-glass substrates covered by a thin TiO_2 dense layer via stationary spin coating deposition. Substrates were cleaned under UV/ozone treatment for 15 min right before the spin coating procedure of the polymer particles suspension. Finally, samples were heated at 70 0C for 30 min in pre-heated oven.

2.5. SYNTHESIS OF THE POROUS TIO_2 FILMS

A $TiCl_4$ 4×10^{-2} M solution in EtOH was deposited on the PS beads-covered substrates by 4-repeated stationary spin coating at 500 RPM for 30 s with a stabilization step at 70 °C for 30 min between each layer. A final calcination step was performed at 500 °C for 30 min (100 °C/h) under air for pristine PS particles or under N_2 for PS-PAN and PS-PDA core-shell particles to remove the beads, crystallize anatase and produce conductive carbon for the last two samples (PS-PAN and PS-PDA).

3. Results and discussion

The general strategy for the TiO_2 film processing is represented in Figure 1 and consists in different steps. First, PS beads as well as PS-PAN and PS-PDA core-shell particles, synthesized by emulsion polymerization, were deposited onto the glass substrates. Then, the TiO_2 precursor was infiltrated

Published in : Colloids and Surfaces A: Physicochemical and Engineering Aspects (2020), vol. 606, 125390
DOI: https://doi.org/10.1016/j.colsurfa.2020.125390
Status : Postprint (Author's version)

in the interstices of the micrometric layers of templating particles which were finally eliminated through calcination. Voids were created in the TiO_2 films as a result of the thermal degradation of the PS core whereas carbon was generated at the surface of TiO_2 via calcination of PAN or PDA. Each step is described and discussed in the next sections followed by a preliminary assessment of the charge transfer properties of the various films.

3.1. SYNTHESIS AND CHARACTERIZATION OF THE POLYMER PARTICLES

Three types of particles with narrow size distribution (Table 1) were considered as templating agents for structuring the TiO_2 films, i.e. PS particles as benchmark materials, as well as PS-PAN and PS-PDA coreshell particles. Figure 2 depicts the general synthesis strategies.

The PS particles were produced via surfactant free emulsion polymerization of styrene initiated by KPS at 70 °C, following a procedure inspired from a previous report [38]. The DLS analysis of the as-prepared particles indicated an average diameter of 354 ± 115 nm (Table 1). TEM images confirmed the size range (~360 nm) of the PS particles as well as their narrow size distribution (Figure 3). A quite similar approach was used for the synthesis of the PS-PAN particles except that styrene and acrylonitrile were added in a sequential manner within the reaction mixture following a procedure described by Yasuda et al. [39]. In the pre-polymerization step, styrene is polymerized alone before addition of AN leading the formation of the PAN shell [39]. Monodispersed PS-PAN particles with an average diameter of about 398 ± 33 nm (Table 1) were obtained accordingly. Finally, the monodisperse PS particles prepared by the surfactant free emulsion polymerization were used as templates for the preparation of PS-PDA core-shell particles. Inspired by a previously reported method [40,41], the coating of the PS particles with PDA was achieved via self-polymerization of dopamine in a weakly alkaline aqueous environment (pH = 8.5) in a Tris-HCl buffer. Compared to the pristine PS particles, a slight increase of the diameter was observed by DLS after the DA condensation (379 ± 81 nm, Table 1), as expected for the formation of the core-shell particles. TEM analysis confirmed that the PS-PDA particles preserved their spherical character as well as the absence of aggregation phenomenon (Figure 3).

All types of particles were subjected to a thermal treatment under N_2 atmosphere in athermogravimetric instrument (TGA) in order to quantify the formation of carbon. In practice, polymer samples were heated at 150 °C for 10 min followed by the increase of temperature to 600 °C at a rate of 20 °C/min. Typical TGA curves are presented in Figure S1 and the percentage of residual carbon are mentioned in Table 1. As expected, almost no carbon was found after calcination of PS. On the other hand, about 4 wt. % of carbon was generated from both PS-PAN and PS-PDA core-shell particles, which makes the comparison of their impact on the TiO_2 films relevant (Table 1).

Raman analyses were also performed to characterize the carbon produced by thermal treatment of the PS-PAN and PS-PDA particles (Figure 4). For the sake of the comparison, the spectrum recorded in identical operating conditions for an electrochemistry grade graphitic carbon is also presented. The G band belongs to the E_{2g} symmetry in plan for graphite and the D band corresponds to the sp^3 carbon. These two bands strongly overlap with other Raman bands observed for disordered carbon also shown in Figure 4, namely the I band belonging to the vibration of sp^2-sp^3 carbon-carbon bond,

Published in : Colloids and Surfaces A: Physicochemical and Engineering Aspects (2020), vol. 606, 125390
DOI: https://doi.org/10.1016/j.colsurfa.2020.125390
Status : Postprint (Author's version)

and both the D' and D'' bands observed for defective graphite systems [42,43]. The D/G intensity ratio relates to the relative content of sp^3 carbons over sp^2 carbons in the carbonaceous materials, hence the D/G intensity ratio decreases when the conductivity of the carbonaceous materials increases. In order to estimate the intensities of the D and G bands and characterize the D/ G ratios of the samples, the Raman spectra were decomposed and the band intensities are listed in Table 2. As expected, the residues of the carbonized PS-PAN and PS-PDA samples present a significant amount of conductive carbon (D/G ratio of 1.38 and 1.36, respectively).

***Table 1**. Characteristics of PS, PS-PAN and PS-PDA particles.*

Particles	DLS diameter ± SD [a] (nm)	TEM average diameter (nm)	Residual carbon [b] (%)
PS	354 ± 115	360	0.33
PS-PAN	398 ± 33	410	3.97
PS-PDA	379 ± 81	370	4.07

a SD stands for standard deviation.

b Residual carbon determined by TGA after thermal treatment at 150 °C for 10 min followed by a temperature ramp between 25 °C and 600 °C (20 °C/min).

***Figure 2**. Synthesis strategies for PS, PS-PAN and PS-PDA particles.*

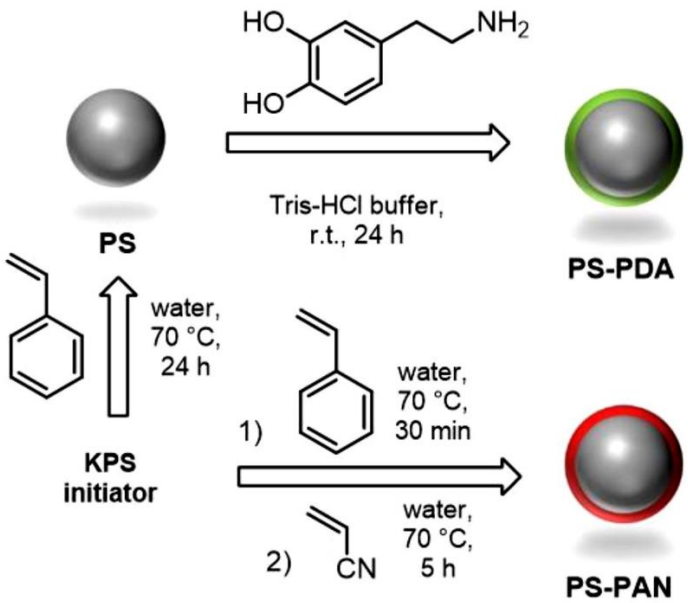

Published in : Colloids and Surfaces A: Physicochemical and Engineering Aspects (2020), vol. 606, 125390
DOI: https://doi.org/10.1016/j.colsurfa.2020.125390
Status : Postprint (Author's version)

***Figure 3**. TEM images of the PS, PS-PAN and PS-PDA particles.*

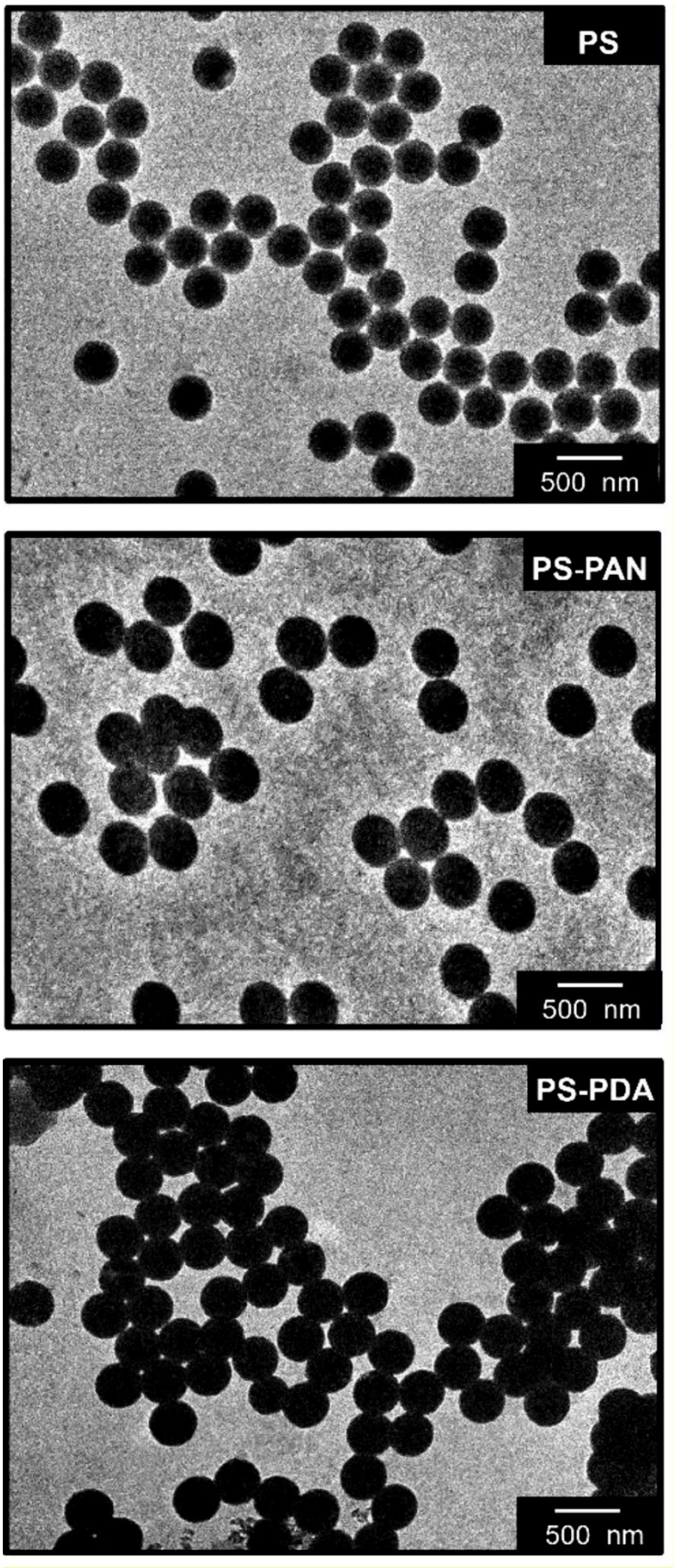

Published in : Colloids and Surfaces A: Physicochemical and Engineering Aspects (2020), vol. 606, 125390
DOI: https://doi.org/10.1016/j.colsurfa.2020.125390
Status : Postprint (Author's version)

***Figure 4**. Raman spectra of carbon generated by thermal degradation of the PS-PAN and PS-PDA particles as well as Raman analysis of electrochemistry-grade graphite.*

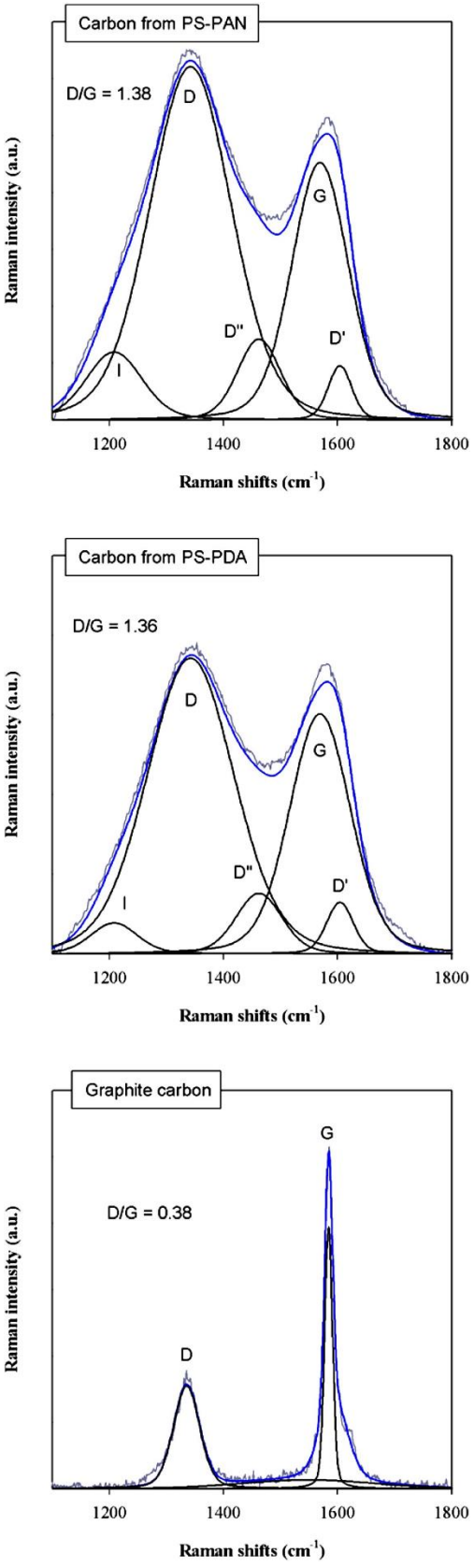

Published in : Colloids and Surfaces A: Physicochemical and Engineering Aspects (2020), vol. 606, 125390
DOI: https://doi.org/10.1016/j.colsurfa.2020.125390
Status : Postprint (Author's version)

***Table 2**. Raman data for the carbonized PS-PAN and PS-PDA as well as for graphite electrode.*

	I ($1225\ cm^{-1}$)	D ($1349\ cm^{-1}$)	D" ($1485\ cm^{-1}$)	G ($1573\ cm^{-1}$)	D' ($1608\ cm^{-1}$)	D/G
PS-PAN	264	1437	317	1043	216	1.38
PS-PDA	476	1544	561	1132	408	1.36
Graphite		434		1156		0.38

3.2. COLLOIDAL ASSEMBLY OF THE PARTICLE TEMPLATES AND PREPARATION OF POROUS TIO_2 FILMS

According to the general strategy depicted by Figure 1, multilayers of particles were formed at the surface of conductive glass, followed by infiltration of the TiO_2 precursor in the interstices of the particles and carbonization. In the case of PDA and PAN core-shell particles, we expect some residual presence of carbon at the surface of the porous TiO_2.

The spin-coating approach is particularly straightforward to this respect and was thus selected for depositing our PS, PS-PAN and PS-PDA particles on FTO-glass. Top view as well as cross sectional SEM images of the resulting spin coated PS, PS-PAN and PS-PDA particles are shown in Figure 5. Whatever the nature of the particles, homogeneous and micrometric layers were obtained. In the case of PS particles, the thickness of the film reached about 2 µm and the particles tend to adopt a closed packed structure characterized by some defects. Similar film thickness and organization were observed for the deposited PS-PAN core-shell particles. In contrast, the PS-PDA particles essentially led to homogeneous but disorganized films which further emphasizes the crucial impact of the particles interactions on the film formation process. In the latter case, however, the substrate was also covered in a quite uniform manner and the thickness of the films was around 1 µm.

Next, a $TiCl_4$ solution in ethanol was infiltrated in the interstices of these polymer particles layers and transformed into TiO_2 upon thermal treatment. Thermal degradation of the PS core of the particles will generate the porosity within the films whereas the PAN or the PDA shells should produce carbon at the surface of the TiO_2. After infiltration of TiCl4 and calcination, the desired inverse opal porous TiO_2 structures with a thickness of about 1 µm were obtained when using the PS and PS-PAN particles as templates. Some cracks were observed in these cases, most probably as a result of the film thermal contraction. Note that the thickness of the polymer particles films was deliberately designed to be larger than the desired thickness of the resulting TiO_2 porous layers. Indeed, the template is only partially filled by the TiO_2 precursor to avoid the formation of a dense crust on top of the porous network, which would, i.a., impede electrolyte infiltration. As illustrated in Figure S2, TEM analysis of the TiO_2 films templated by the PS-PAN particles tends to confirm the presence of a thin layer (~ 4 nm) of carbon at the surface of the TiO_2 cavities. On the other hand, SEM

Published in : Colloids and Surfaces A: Physicochemical and Engineering Aspects (2020), vol. 606, 125390
DOI: https://doi.org/10.1016/j.colsurfa.2020.125390
Status : Postprint (Author's version)

images of the TiO_2 layer obtained from the PS-PDA beads show a completely different film morphology that essentially consists in a disordered deposit presenting some spherical cavities (see the bottom picture in Figure 6). This disorganization might be due to specific interactions between the PDA and TiO_2 or by reaction of the former with the $TiCl_4$ precursor during the infiltration step. According to a previous study, the abundant catechol groups of PDA [44] are likely to bind Ti compounds [45], which seems to affect the formation of the TiO_2 inverse opals in the present case. Regardless of the nature of the outershell of the particles, however, Raman spectroscopy confirmed the formation of conductive carbon and anatase TiO_2, as discussed below.

Figure 5*. SEM images of the top surface and cross section of spin coated PS, PS-PAN and PS-PDA particles onto FTO glass.*

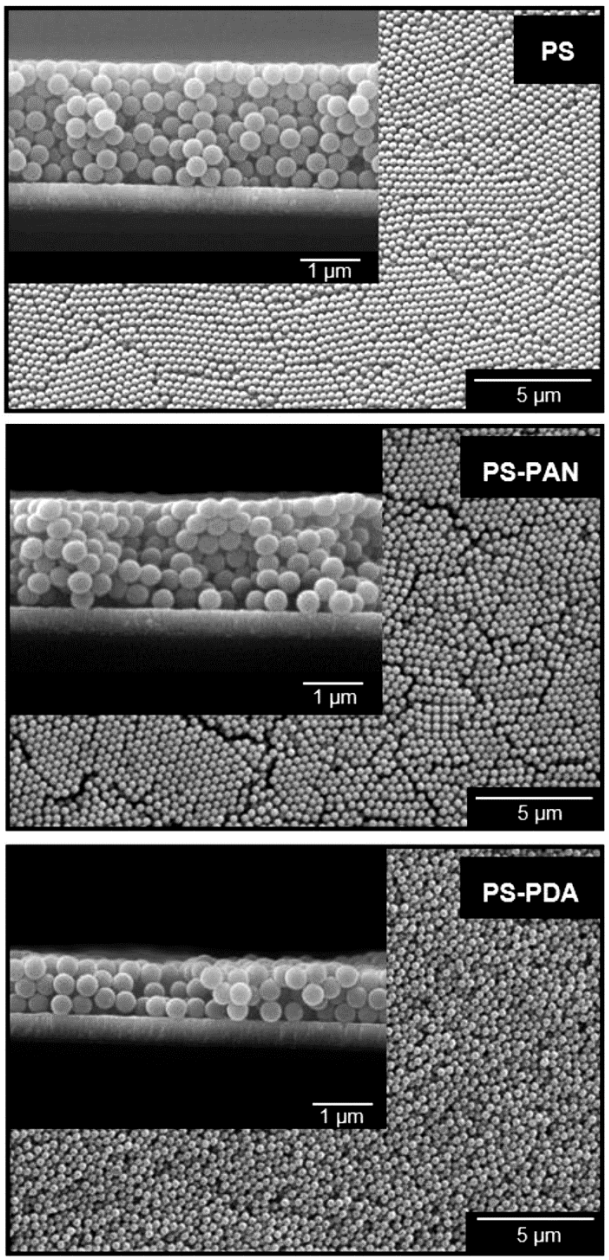

Published in : Colloids and Surfaces A: Physicochemical and Engineering Aspects (2020), vol. 606, 125390
DOI: https://doi.org/10.1016/j.colsurfa.2020.125390
Status : Postprint (Author's version)

3.3. RAMAN AND EIS CHARACTERIZATION OF THE POROUS TIO_2 FILMS

The TiO_2 porous films templated by PS, PS-PAN and PS-PDA particles were first analyzed by Raman spectroscopy in order to determine the nature of the TiO_2 formed and detect the presence of conductive carbon within the films (Figure 7). Raman data are summarized in Table 3. Regardless of the nature of the particles used as template, a dominant band around 142 cm^{-1} indicates that TiO_2 mainly consists in anatase, a polymorph of particular interest for photoelectrochemical applications thanks notably to its large bandgap and high charge carrier mobility [46]. However, in the case of PS-PAN, the band is broaden and slightly shifted to 144 cm^{-1}. This indicates an amorphization of the TiO_2 film, which is further established from XRD measurements (Figure S3). Raman spectroscopy and XRD also rule out the presence of rutile phase. Indeed, the characteristic TiO_2 rutile (110) peak at 27.4° is not observed in the XRD spectrum (Figure S3) and the Raman spectrum presented in Figure 7 does not show the characteristic bands of rutile at 445 and 610 cm^{-1}.

In the extended Raman spectra of the TiO_2 films templated by PS-PAN and PS-PDA particles, the characteristic G and D bands are clearly observed, belonging respectively to the E_{2g} symmetry in plan C-C stretching occurring in sp^2 systems and to the A_{1g} symmetry breathing of the six-fold ring of C-C bond observed for disordered carbon due to out of plane vibrations of sp^3 systems. The relative intensities of these bands (D/G ratio) suggest that calcination of the PS-PDA (1.30) produced, at the surface of TiO_2, a sp2 carbon atoms bonded system with less structural defects, and so more conductive, compared to PS-PAN (1.49).

Finally, Electrochemical Impedance Spectroscopy (EIS) analyses were carried out to assess the influence of the carbon at the surface of the TiO_2 porous layers in terms of charge transfer for potential photoanode application. A liquid electrolyte medium consisting of $TBAClO_4$ dissolved in CH_2Cl_2 was used here to assure sufficient degree of penetration and impregnation into the different porous TiO_2 networks (which was established from naked-eye observations of the spreading of a drop of electrolyte on the electrodes surfaces). Other liquid media were tried, including aqueous ones, but none were shown to be efficient in this respect, especially with the carbon-containing layers. Figure 8a shows typical Nyquist plots measured for the different cases with the abovementioned carbon-coated and non-coated TiO_2 films. The measured electrical values, obtained from EIS data fitting according to a reference equivalent circuit [47-49] shown on Figure 8b, are listed in Table 4.

Overall, the charge transfer resistance (R3) values of the porous TiO_2 layers at the interface with the liquid electrolyte follow the order: TiO_2/PS-PAN < < < TiO_2/PS < TiO_2/PS-PDA. Surprisingly, the lowest charge transfer resistance is observed for the TiO_2 film templated by PS-PAN core-shell particles despite a higher amount of structural defects in the sp2 carbon atoms bonded system and a less crystallized anatase structure compared to TiO_2/PS-PDA, as previously established from Raman analyses. The trend of charge transfer resistance at the TiO_2 electrode/electrolyte interface is further corroborated by the extent of charge diffusion from the bulk electrolyte to the electrode. This aspect is quantified by the W4 values, shown to increase progressively from TiO_2/PS-PDA to TiO_2/PS and even further to TiO_2/ PS-PAN. Regarding the charge transfer behavior at the counter electrode, it seems

Published in : Colloids and Surfaces A: Physicochemical and Engineering Aspects (2020), vol. 606, 125390
DOI: https://doi.org/10.1016/j.colsurfa.2020.125390
Status : Postprint (Author's version)

to be facilitated in the case of carbon-coated TiO_2 working electrodes (lower R2 values for TiO_2/PS-PAN and TiO_2/PS-PDA) than with non-carbon-coated ones (higher R2 value for TiO_2/PS).

The combination of a good quality of structural organization and a conductive character is thus crucial, and explains why the TiO_2/PS-PAN layer is ultimately the most promising system in terms of interfacial conductivity. In contrast, the lower charge transfer performances observed for the films templated by PS-PDA particles seem mostly caused by the very poor organization of the porous network (cf. SEM micrographs presented in Figure 6), rather acting here as a barrier layer to charge transfers between the TiO_2 layer and the electrolyte. Interestingly, the charge transfer resistance of the TiO_2/PS benchmark is also lower than the TiO_2/PS-PDA case, thanks to its better porous organization, but still higher than the TiO_2/PS-PAN case because of its less conductive nature in absence of carbon material.

***Figure 6**. SEM images of the top surface and cross section of the TiO_2 porous films templated by PS, PS-PAN and PS-PDA particles.*

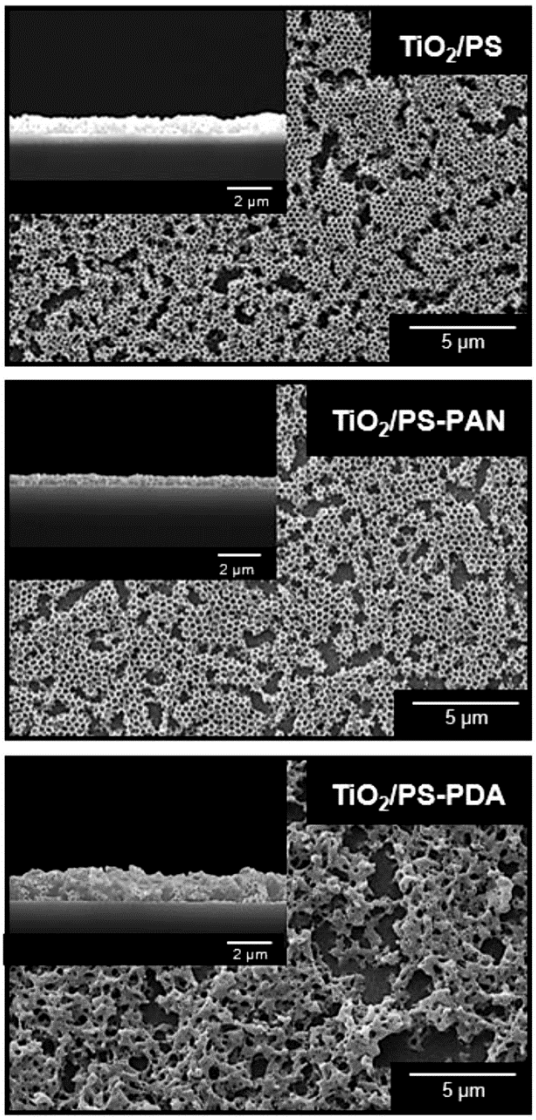

Published in : Colloids and Surfaces A: Physicochemical and Engineering Aspects (2020), vol. 606, 125390
DOI: https://doi.org/10.1016/j.colsurfa.2020.125390
Status : Postprint (Author's version)

***Figure 7**. Raman spectra for the TiO_2 porous films templated by PS, PS-PAN and PS-PDA particles.*

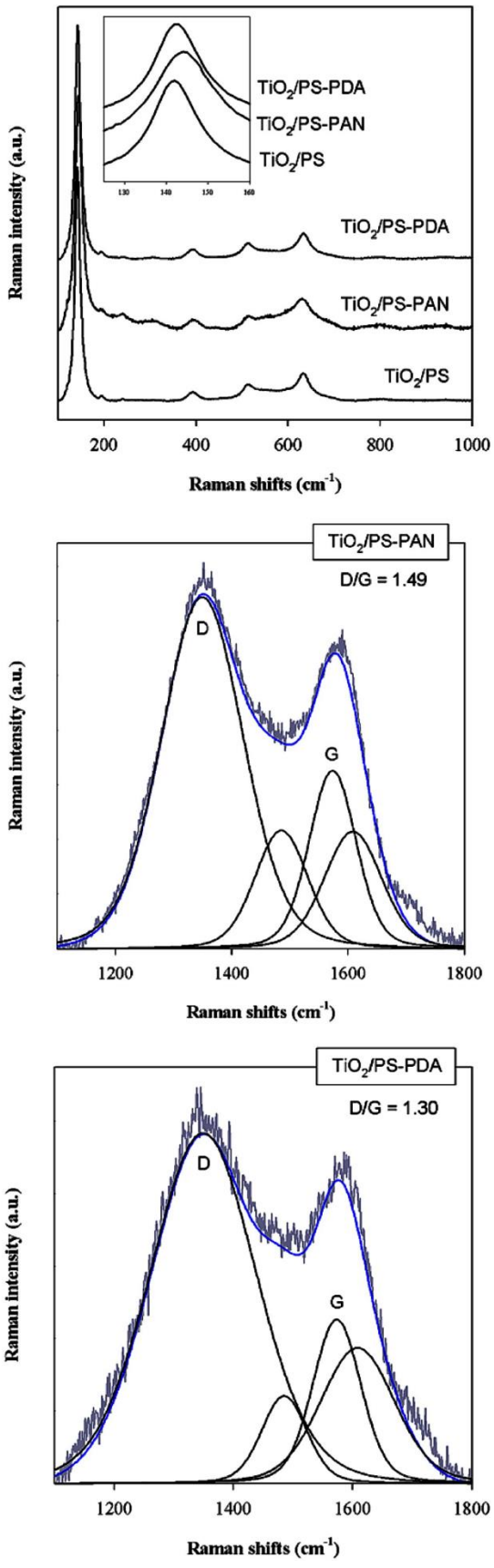

Published in : Colloids and Surfaces A: Physicochemical and Engineering Aspects (2020), vol. 606, 125390
DOI: https://doi.org/10.1016/j.colsurfa.2020.125390
Status : Postprint (Author's version)

***Table 3**. Raman intensities for the TiO_2 porous films templated by PS-PAN and PS-PDA particles.*

TiO_2 films	TiO_2 Band position ± SD (cm^{-1})	D (1349 cm^{-1})	D" (1485 cm^{-1})	G (1573 cm^{-1})	D' (1608 cm^{-1})	D/G
TiO_2/PS-PAN	144.2 ± 0.8	1303	262	874	368	1.49
TiO_2/PS-PDA	142.8 ± 0.2	1060	145	816	404	1.30

***Figure 8**. a) EIS curve for the TiO_2 porous layers templated by PS, PS-PAN and PS-PDA particles. b) Equivalent circuit model for the fitting of the anode [47-49]. R1: contacts; R2 (resistance) & Q2 (capacity): transfers at the counter electrode; R3 & Q3: transfers at interface TiO_2 electrode / electrolyte; W4: diffusion in electrolyte.*

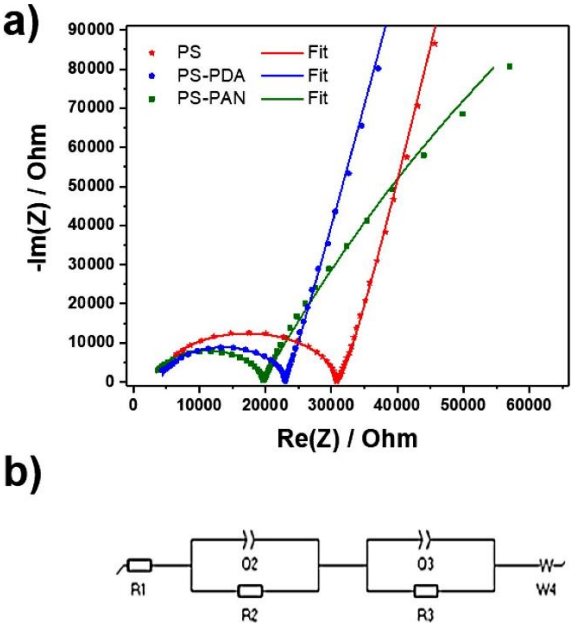

***Table 4**. EIS fitting data obtained from measurements of the TiO_2 porous films templated by PS, PS-PAN and PS-PDA particles.*

TiO_2 films	R1 (Ohm)	R2 (Ohm)	Q2 (F.s)	R3 (Ohm)	Q3 (F.s)	W4 ($Ohm.s^{-1/2}$)
TiO_2/PS	3552	27,365	3.4 E-11	1.1 E+8	5.2 E-6	7463
TiO_2/PS-PAN	3107	16,130	3.2 E-11	7.0 E+5	1.5 E-6	15,594
TiO_2/PS-PDA	4236	18,659	8.4 E-11	1.3 E+9	4.5 E-6	3841

Published in : Colloids and Surfaces A: Physicochemical and Engineering Aspects (2020), vol. 606, 125390
DOI: https://doi.org/10.1016/j.colsurfa.2020.125390
Status : Postprint (Author's version)

4. Conclusion

Monodisperse PS particles as well as PS-PAN and PS-PDA core-shell particles were synthesized by emulsion polymerization methods and used as templates for the preparation of porous TiO_2 layers. The spin coating deposition of the PS and the PS-PAN particles led to organized micrometric colloidal films, whereas disordered layers were obtained in the case of the PS-PDA particles. After infiltration of $TiCl_4$ in the interstices of the different particle layers and carbonization, inverse opal porous anatase TiO_2 structures were only achieved by using the PS and PS-PAN templates whereas PS-PDA led to disordered films. As expected, conductive carbon was detected by Raman at the surface of the porous TiO_2 films templated by the core-shell particles as a result of the carbonization of the PAN and PDA phases. Crucially, Electrochemical Impedance Spectroscopy (EIS) was used so to establish and quantify the semiconducting properties of the various sorts of TiO_2 electrodes. The lowest interfacial resistivity was measured for the porous TiO_2 film templated by the PS-PAN particles, thanks to the beneficial synergic effect of a combined ordered porosity and conductive carbon coating. In comparison, the carbon produced from the PS-PDA particles, despite being intrinsically more conductive, cannot compensate the less ordered nature of the resulting TiO_2 porous film, which ultimately alters the interfacial charge transfer properties of the latter and leads to an increased charge transfer resistivity at the TiO_2 electrode/electrolyte interface, as established from EIS. Overall, using PS-PAN core-shell particles as templating agents and source of carbon is therefore a promising and straightforward approach to improve the performances of TiO_2 porous films in optoelectronic and photoelectrochemical materials.

CRediT authorship contribution statement

Vidhyadevi Thangaraj: Conceptualization, Validation, Investigation, Writing - original draft, Writing - review & editing. Jennifer Dewalque: Conceptualization, Validation, Investigation, Writing - original draft, Writing - review & editing, Project administration, Funding acquisition. Anthony Maho: Conceptualization, Validation, Investigation, Writing - original draft, Writing - review & editing. Gilles Spronck: Investigation, Validation. Cédric Malherbe: Investigation, Writing - original draft, Writing - review & editing. Abdelhafid Aqil: Investigation, Writing - review & editing. Rudi Cloots: Conceptualization, Writing - review & editing, Supervision, Funding acquisition. Pierre Colson: Conceptualization, Writing - review & editing, Supervision, Project administration, Funding acquisition. Christine Jérôme: Conceptualization, Writing - review & editing, Supervision, Funding acquisition. Antoine Debuigne: Conceptualization, Visualization, Writing - original draft, Writing - review & editing, Supervision, Project administration, Funding acquisition.

Acknowledgments

The research was funded by the Walloon Region, Belgium, through the SOLIDYE_1 Project (Complement FEDER, Grant agreement 1510607). The authors are grateful to the Belgian National Funds for Scientific Research (F.R.S.-FNRS) for their financial support; C.M. and A.D. are FNRS Post-doctoral Researcher and Research Associate, respectively. The authors also thank A. Schrijnemakers (GREEnMat) and M. Dejeneffe (CERM) for their skillful assistance.

Appendix A. Supplementary data

Supplementary material related to this article can be found, in the online version, at doi: https://doi.org/10.1016/j.colsurfa.2020.125390

Published in : Colloids and Surfaces A: Physicochemical and Engineering Aspects (2020), vol. 606, 125390
DOI: https://doi.org/10.1016/j.colsurfa.2020.125390
Status : Postprint (Author's version)

Supplementary Material

***Figure S1**. TGA curves recorded under nitrogen for the PS, PS-PAN and PS-PDA particles. Residual carbon of 0.33%, 3.97% and 4.07% are respectively determined for PS, PS-PAN and PS-PDA particles.*

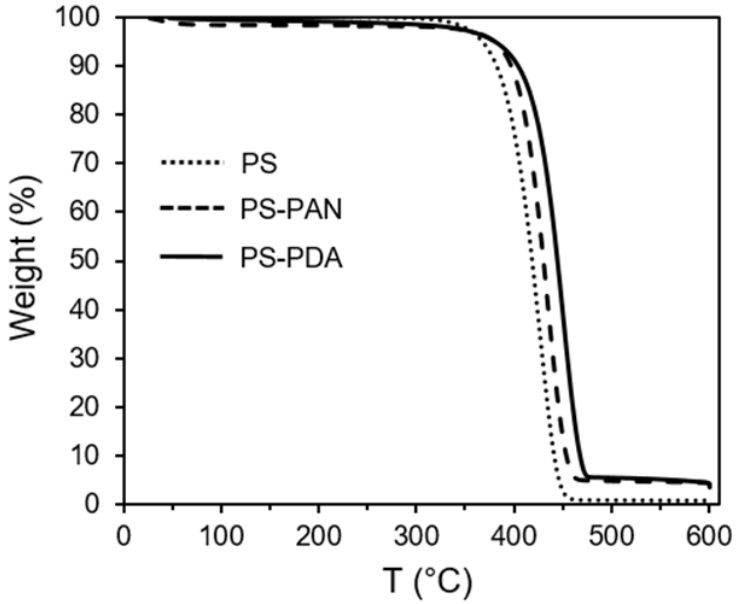

***Figure S2**. TEM image of the TiO_2 film templated by PS-PAN particles, emphasizing the presence of a thin layer (~ 4 nm) of carbon at the surface of the TiO_2 cavities.*

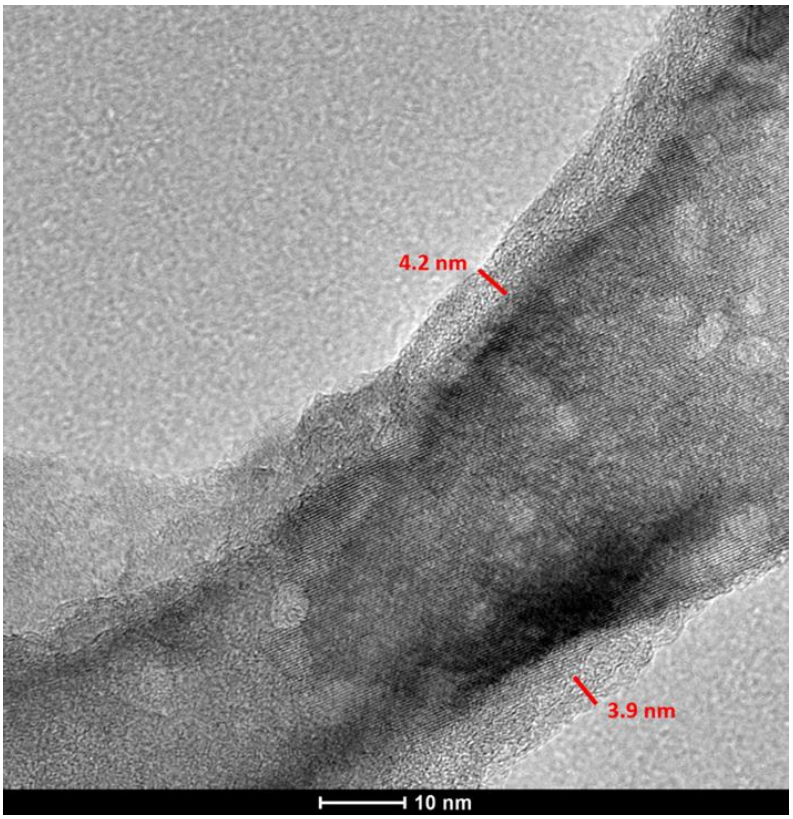

Published in : Colloids and Surfaces A: Physicochemical and Engineering Aspects (2020), vol. 606, 125390
DOI: https://doi.org/10.1016/j.colsurfa.2020.125390
Status : Postprint (Author's version)

***Figure S3**. X-ray diffractograms of the TiO_2 porous films templated by PS-PDA and PS-PAN particles. The drop of intensity observed for the (101) TiO_2 anatase peak at 25.3° on the TiO_2/PS-PAN sample (in comparison with the TiO_2/PS-PDA sample) is correlated to an amorphization of the corresponding TiO_2 film. The presence of rutile is ruled out as the characteristic (110) TiO_2 rutile peak at 27.4° is not observed.*

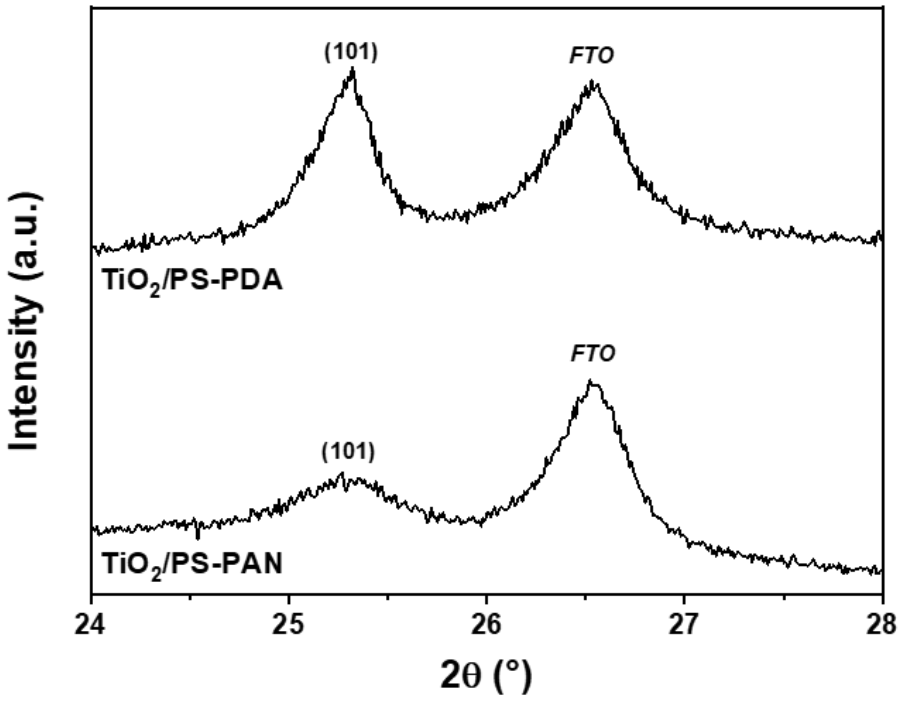

Published in : Colloids and Surfaces A: Physicochemical and Engineering Aspects (2020), vol. 606, 125390
DOI: https://doi.org/10.1016/j.colsurfa.2020.125390
Status : Postprint (Author's version)

References

[1] N.A. Ludin, A.M.A. Mahmoud, A. Bakar, A. Amir, H. Kadhum, K. Sopian, N. Shazlinah, A. Karim, Review on the development of natural dye photosensitizer for dye-sensitized solar cells, Renew. Sustain. Energy Rev. 31 (2014) 386–396, https://doi.org/10.1016/j.rser.2013.12.001.

[2] M. Fehse, E. Ventosa, Is TiO 2 (B) the future of titanium-based battery materials? Chem Plus Chem. 80 (2015) 785–795, https://doi.org/10.1002/cplu.201500038.

[3] R. Fagan, D.E. McCormack, D.D. Dionysiou, S.C. Pillai, A review of solar and visible light active TiO_2 photocatalysis for treating bacteria, cyanotoxins and contaminants of emerging concern, Mater. Sci. Semicond. Process. 42 (2016) 2–14, https://doi.org/10.1016/j.mssp.2015.07.052.

[4] J. Schneider, M. Matsuoka, M. Takeuchi, J. Zhang, Y. Horiuchi, M. Anpo, D.W. Bahnemann, Understanding TiO_2 photocatalysis: mechanisms and materials, Chem. Rev. 114 (2014) 9919–9986, https://doi.org/10.1021/cr5001892.

[5] J. Bai, B. Zhou, Titanium dioxide nanomaterials for sensor applications, Chem. Rev. 114 (2014) 10131–10176, https://doi.org/10.1021/cr400625j.

[6] S. Sun, P. Song, J. Cui, S. Liang, Amorphous TiO_2 nanostructures: synthesis, fundamental properties and photocatalytic applications, Catal. Sci. Technol. 9 (2019) 4198–4215, https://doi.org/10.1039/C9CY01020C.

[7] W. Kim, S.Y. Choi, Y.M. Jeon, S. Lee, S.H. Kim, Highly ordered, hierarchically porous TiO_2 films via combination of two self-assembling templates, ACS Appl. Mater. Interfaces 6 (2014) 11484–11492, https://doi.org/10.1021/am502137d.

[8] S.-C. Yang, D.-J. Yang, J. Kim, J.-M. Hong, H.-G. Kim, I.-D. Kim, H. Lee, Hollow TiO_2 hemispheres obtained by colloidal templating for application in dye-sensitized solar cells, Adv. Mater. 20 (2008) 1059–1064, https://doi.org/10.1002/adma.200701808.

[9] P. Colson, C. Henrist, R. Cloots, Nanosphere lithography : a powerful method for the controlled manufacturing of nanomaterials, J. Nanomater. (2013) ID 948510.

[10] V. Jovic, H. Idriss, G.I.N. Waterhouse, Slow photon amplification of gas-phase ethanol photo-oxidation in titania inverse opal photonic crystals, Chem. Phys. 479 (2016) 109–121, https://doi.org/10.1016/j.chemphys.2016.10.001.

[11] N. Vogel, M. Retsch, C.-A. Fustin, A. del Campo, U. Jonas, Advances in colloidal assembly: the design of structure and hierarchy in two and three dimensions, Chem. Rev. 115 (2015) 6265–6311, https://doi.org/10.1021/cr400081d.

[12] J. Yu, J. Lei, L. Wang, J. Zhang, Y. Liu, TiO_2 inverse opal photonic crystals: synthesis, modification, and applications - a review, J. Alloys Compd. 769 (2018) 740–757, https://doi.org/10.1016/j.jallcom.2018.07.357.

[13] E. Armstrong, C. O'Dwyer, Artificial opal photonic crystals and inverse opal structures – fundamentals and applications from optics to energy storage, J. Mater. Chem. C 3 (2015) 6109–6143, https://doi.org/10.1039/C5TC01083G.

[14] J.-H. Shin, J.-H. Kang, W.-M. Jin, J.H. Park, Y.-S. Cho, J.H. Moon, Facile synthesis of TiO_2 inverse opal electrodes for dye-sensitized solar cells, Langmuir 27 (2011) 856–860, https://doi.org/10.1021/la104512c.

[15] J.W. Lee, J. Lee, C. Kim, C.-Y. Cho, J.H. Moon, Facile fabrication of sub-100 nm mesoscale inverse opal films and their application in dye-sensitized solar cell electrodes, Sci. Rep. 4 (2014) 6804, https://doi.org/10.1038/srep06804.

[16] A.K. Bharwal, L. Manceriu, F. Alloin, C. Iojoiu, J. Dewalque, T. Toupance, C. Henrist, Tuning bimodal porosity in TiO_2 photoanodes towards efficient solidstate dye-sensitized solar cells comprising polysiloxane-based polymer electrolyte, Microporous Mesoporous Mater. 273 (2019) 226–234, https://doi.org/10.1016/j.micromeso.2018.07.013.

[17] A.K. Bharwal, L. Manceriu, F. Alloin, C. Iojoiu, J. Dewalque, T. Toupance, C. Henrist, Bimodal titanium oxide photoelectrodes with tuned porosity for improved light harvesting and polysiloxane-based polymer electrolyte infiltration, Sol. Energy 178 (2019) 98–107, https://doi.org/10.1016/j.solener.2018.12.030.

[18] J. Zhong, F. Chen, J. Zhang, Carbon-deposited TiO_2: synthesis, characterization, and visible photocatalytic performance, J. Phys. Chem. C 114 (2010) 933–939, https://doi.org/10.1021/jp909835m.

[19] M. Madian, A. Eychmüller, L. Giebeler, Current advances in TiO_2-based nanostructure electrodes for high performance lithium ion batteries, Batteries 4 (2018) 7, https://doi.org/10.3390/batteries4010007.

[20] J.U. Ha, J. Lee, M.A. Abbas, M.D. Lee, J. Lee, J.H. Bang, Designing hierarchical assembly of carbon-coated TiO_2 nanocrystals and unraveling the role of TiO_2/carbon interface in lithium-ion storage in TiO_2, ACS Appl. Mater. Interfaces 11(2019) 11391–11402, https://doi.org/10.1021/acsami.8b21705.

[21] H. Abdullah, M.Z. Razali, S. Shaari, M.R. Taha, Enhancement of dye-sensitized solar cell efficiency using carbon nanotube/TiO_2 nanocomposite thin films fabricated at various annealing temperatures, Electron. Mater. Lett. 10 (2014) 611–619, https://doi.org/10.1007/s13391-013-3132-0.

[22] T.Y. Lee, P.S. Alegaonkar, J.-B. Yoo, Fabrication of dye sensitized solar cell using TiO_2 coated carbon nanotubes, Thin Solid Films 515 (2007) 5131–5135, https://doi.org/10.1016/j.tsf.2006.10.056.

[23] M.N. Tahir, B. Oschmann, D. Buchholz, X. Dou, I. Lieberwirth, M. Panthöfer, W. Tremel, R. Zentel, S. Passerini, Extraordinary performance of carbon-coated anatase TiO_2 as sodium-ion anode, Adv. Energy Mater. 6 (2016) 1501489, , https://doi.org/10.1002/aenm.201501489.

[24] W. Devina, D. Nam, J. Hwang, C. Chandra, W. Chang, J. Kim, Carbon-coated, hierarchically mesoporous TiO_2 microparticles as an anode material for lithium and sodium ion batteries, Electrochim. Acta 321 (2019) 134639, , https://doi.org/10.1016/j.electacta.2019.134639.

[25] G. Odling, A. Ivaturi, E. Chatzisymeon, N. Robertson, Improving carbon-coated TiO_2 films with a $TiCl_4$ treatment for photocatalytic water purification, ChemCatChem 10 (2018) 234–243, https://doi.org/10.1002/cctc.201700867.

[26] T. Zeng, P. Ji, X. Hu, G. Li, Nano-Sn doped carbon-coated rutile TiO_2 spheres as a high capacity anode for Li-ion battery, RSC Adv. 6 (2016) 48530–48536, https://doi.org/10.1039/C6RA04672J.

[27] M.A. Nawi, I. Nawawi, Preparation and characterization of TiO_2 coated with a thin carbon layer for enhanced photocatalytic activity under fluorescent lamp and solar light irradiations, Appl. Catal. A Gen. 453 (2013) 80–91, https://doi.org/10.1016/j.apcata.2012.11.047.

[28] M.S.A. Rahaman, A.F. Ismail, A. Mustafa, A review of heat treatment on polyacrylonitrile fiber, Polym. Degrad. Stab. 92 (2007) 1421–1432, https://doi.org/10.1016/j.polymdegradstab.2007.03.023.

Published in : Colloids and Surfaces A: Physicochemical and Engineering Aspects (2020), vol. 606, 125390
DOI: https://doi.org/10.1016/j.colsurfa.2020.125390
Status : Postprint (Author's version)

[29] C. Kim, S. Park, J. Cho, D. Lee, T. Park, W. Lee, K. Yang, Raman spectroscopic evaluation of polyacrylonitrile-based carbon nanofibers prepared by electrospinning, J. Raman Spectrosc. (2004) 928–933, https://doi.org/10.1002/jrs.1233.

[30] P. Bajaj, A.K. Roopanwal, Thermal stabilization of acrylic precursors for the production of carbon fibers : an overview, J. Macromol. Sci. Part C Polym. Rev. (1997) 97–147, https://doi.org/10.1080/15321799708014734.

[31] L.C. Yang, Y. Shi, Q.S. Gao, B. Wang, Y.P. Wu, Y. Tang, The production of carbon nanospheres by the pyrolysis of polyacrylonitrile, Carbon 6 (2008) 1816–1818, https://doi.org/10.1016/j.carbon.2008.07.012.

[32] J. Thomassin, A. Debuigne, C. Jérôme, C. Detrembleur, Design of mesoporous carbon fi bers from a poly (acrylonitrile) based block copolymer by a simple templating compression moulding process, Polymer 51 (2010) 2965–2971, https://doi.org/10.1016/j.polymer.2010.05.010.

[33] W. Zhou, X. Xiao, M. Cai, L. Yang, Polydopamine-coated, nitrogen-doped, hollow carbon − sulfur double-layered core − shell structure for improving lithium − sulfur batteries, Nano Lett. (2014) 5250–5256, https://doi.org/10.1021/nl502238b.

[34] J. Kong, W.A. Yee, L. Yang, Y. Wei, S.L. Phua, H.G. Ong, J.M. Ang, X. Li, X. Lu, Highly electrically conductive layered carbon derived from polydopamine and its functions in SnO_2-based lithium ion battery anodes, Chem. Commun. 48 (2012) 10316–10318, https://doi.org/10.1039/C2CC35284B.

[35] X. Yu, H. Fan, Y. Liu, Z. Shi, Z. Jin, Characterization of carbonized polydopamine nanoparticles suggests ordered supramolecular structure of polydopamine, Langmuir (2014) 5497–5505, https://doi.org/10.1021/la500225v.

[36] C. Lei, F. Han, D. Li, W.-C. Li, Q. Sun, X.-Q. Zhang, A.-H. Lu, Dopamine as the coating agent and carbon precursor for the fabrication of N-doped carbon coated Fe3O4 composites as superior lithium ion anodes, Nanoscale 5 (2013) 1168–1175, https://doi.org/10.1039/C2NR33043A.

[37] R. Liu, S.M. Mahurin, C. Li, R.R. Unocic, J.C. Idrobo, H. Gao, S.J. Pennycook, S. Dai, Dopamine as a carbon source : the controlled synthesis of hollow carbon spheres and yolk-structured carbon nanocomposites, Angew. Chem. (2011) 6799–6802, https://doi.org/10.1002/anie.201102070.

[38] Z. Cai, J. Teng, Q. Yan, X.S. Zhao, Solvent effect on the self-assembly of colloidal microspheres via a horizontal deposition method, Colloids Surf. A Physicochem. Eng. Asp. 402 (2012) 37–44, https://doi.org/10.1016/j.colsurfa.2012.03.015.

[39] H. Tamai, T. Sumi, H. Yasuda, Preparation and characteristics of fine hollow carbon particles, J. Colloid Interface Sci. 177 (1996) 325–328, https://doi.org/10.1006/jcis.1996.0038.

[40] Y. Wang, B. Shang, M. Liu, F. Shi, B. Peng, Z. Deng, Hollow polydopamine colloidal composite particles: structure tuning, functionalization and applications, J. Colloid Interface Sci. 513 (2018) 43–52, https://doi.org/10.1016/j.jcis.2017.10.102.

[41] M. Kohri, Y. Nannichi, H. Kohma, D. Abe, T. Kojima, T. Taniguchi, K. Kishikawa, Aspects Size control of polydopamine nodules formed on polystyrene particles during dopamine polymerization with carboxylic acid-containing compounds for the fabrication of raspberry-like particles, Colloids Surf. A Physicochem. Eng. Asp. 449 (2014) 114–120, https://doi.org/10.1016/j.colsurfa.2014.02.049.

[42] L. Bokobza, J.-L. Bruneel, M. Couzi, Raman Spectra of carbon-based materials (from graphite to carbon black) and of some silicone composites, C — J. Carbon Res. 1 (2015) 77–94, https://doi.org/10.3390/c1010077.

[43] Y. Wang, D.C. Alsmeyer, R.L. McCreery, Raman spectroscopy of carbon materials: structural basis of observed spectra, Chem. Mater. 2 (1990) 557–563, https://doi.org/10.1021/cm00011a018.

[44] J. Liebscher, R. Mrówczyński, H.A. Scheidt, C. Filip, N.D. Hădade, R. Turcu, A. Bende, S. Beck, Structure of polydopamine: a never-ending story? Langmuir 29 (2013) 10539–10548, https://doi.org/10.1021/la4020288.

[45] Y. Jiang, K. Shi, H. Tang, Y. Wang, Enhanced wettability and wear resistance on TiO_2/PDA thin films prepared by sol-gel dip coating, Surf. Coatings Technol. 375 (2019) 334–340, https://doi.org/10.1016/j.surfcoat.2019.07.051.

[46] S. Shen, J. Chen, M. Wang, X. Sheng, X. Chen, X. Feng, S.S. Mao, Titanium dioxide nanostructures for photoelectrochemical applications, Prog. Mater. Sci. 98 (2018) 299–385, https://doi.org/10.1016/j.pmatsci.2018.07.006.

[47] M. Adachi, M. Sakamoto, J. Jiu, Y. Ogata, S. Isoda, Determination of parameters of Electron transport in dye-sensitized solar cells using electrochemical impedance spectroscopy, J. Phys. Chem. B 110 (2006) 13872–13880, https://doi.org/10.1021/jp061693u.

[48] C.-P. Hsu, K.-M. Lee, J.T.-W. Huang, C.-Y. Lin, C.-H. Lee, L.-P. Wang, S.-Y. Tsai, K.-C. Ho, EIS analysis on low temperature fabrication of TiO_2 porous films for dyesensitized solar cells, Electrochim. Acta 53 (2008) 7514–7522, https://doi.org/10.1016/j.electacta.2008.01.104.

[49] T. Lopes, L. Andrade, H.A. Ribeiro, A. Mendes, Characterization of photoelectrochemical cells for water splitting by electrochemical impedance spectroscopy, Int. J. Hydrogen Energy 35 (2010) 11601–11608, https://doi.org/10.1016/j.ijhydene.2010.04.001.